Graphical Abstract

Observations of the synthesis of straight single wall carbon nanotubes directed by electric fields in an Environmental Transmission Electron Microscope

Pascal Vincent, Federico Panciera, Ileana Florea, Nicholas Blanchard, Costel Sorin Cojocaru, Mariam Ezzedine, Haifa Taoum, Sorin Perisanu, Pierre De Laharpe, Anthony Ayari, Julien Chaste, Khakimjon Saidov, Utkur Mirsaidov, Stephen Thomas Purcell, Pierre Legagneux

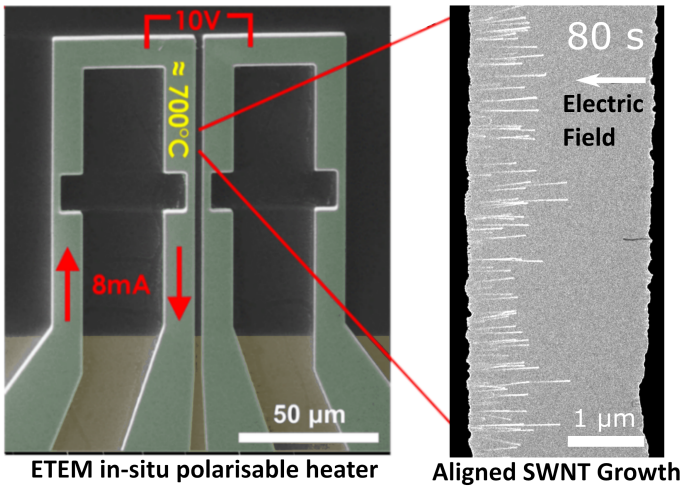

Highlights

Observations of the synthesis of straight single wall carbon nanotubes directed by electric fields in an Environmental Transmission Electron Microscope

Pascal Vincent, Federico Panciera, Ileana Florea, Nicholas Blanchard, Costel Sorin Cojocaru, Mariam Ezzedine, Haifa Taoum, Sorin Perisanu, Pierre De Laharpe, Anthony Ayari, Julien Chaste, Khakimjon Saidov, Utkur Mirsaidov, Stephen Thomas Purcell, Pierre Legagneux

- Electric field directed CVD growth of free-standing single wall carbon nanotubes.
- Real time growth rate measurements using Environmental Transmission Electron Microscope
- Constant growth rate is dominant but other behaviors such as growth acceleration are present
- Depending on voltages Field Emission can appear during growth and even limit the growth.

Observations of the synthesis of straight single wall carbon nanotubes directed by electric fields in an Environmental Transmission Electron Microscope

Pascal Vincent[a,*], Federico Panciera[b,*], Ileana Florea[c,d,*], Nicholas Blanchard[a], Costel Sorin Cojocaru[c], Mariam Ezzedine[c], Haifa Taoum[c], Sorin Perisanu[a], Pierre De Laharpe[e], Anthony Ayari[a], Julien Chaste[b], Khakimjon Saidov[f], Utkur Mirsaidov[f], Stephen Thomas Purcell[a], Pierre Legagneux[e]

[a] *Univ Lyon Univ Claude Bernard Lyon 1 CNRS Institut Lumiere Matiere F-69622 Villeurbanne France.*
[b] *University of Paris-Saclay CNRS Centre for Nanoscience and Nanotechnology 91120 Palaiseau France.*
[c] *Laboratory of Physics of Interfaces and Thin Films UMR CNRS 7647 Ecole Polytechnique IP-Paris 91228 Palaiseau France.*
[d] *Current address : Universite Cote d'Azur CNRS CRHEA 06 905 Sophia Antipolis cedex France.*
[e] *Thales Research and Technology Palaiseau France.*
[f] *Centre for BioImaging Sciences Departments of Physics and Biological Sciences National University of Singapore 14 Science Drive 4 Singapore 117557.*

Abstract

We report here observations in real time of the aligning effect of electric fields during the synthesis of carbon nanotubes in an environmental transmission electron microscope (ETEM). Growths took place using C_2H_2 as precursor gas at $\sim 10^{-4}$ mbar, a temperature of $\sim 700\ ^{\circ}C$ and within a micro-capacitor incorporated in a specifically-designed heating micro-chip. Individual nanotubes are easily resolved as they appear as extremely straight lines growing parallel to the electric field. These nanotubes are predominantly Single Wall Carbon Nanotubes (SWNTs). Owing to the very good alignment of nan-

*Corresponding authors
Email addresses: pascal.vincent@univ-lyon1.fr (Pascal Vincent), federico.panciera@c2n.upsaclay.fr (Federico Panciera), if@crhea.cnrs.fr (Ileana Florea)

otubes in the object plane of the microscope we can obtain unprecedented excellent determination of the nanotubes' growth rates and follow them dynamically. Constant growth rates are observed in most cases but other behaviours are observed such as growth rate acceleration. For low applied voltages the growing nanotubes can cross the gap and connect to the opposite electrode although some are destroyed by mechanical failure or during the contact. For high applied fields and positive biasing allowing Field Emission (FE), the growth is limited within the gap as FE can occur during growth leading to new saturation or destruction processes. These different mechanisms are presented as well as the observed balance between electrostatic and adhesion forces.

Keywords: Single Wall Carbon Nanotubes; Electric Field Directed Growth; Environmental Transmission Microscope; Growth kinetics; Nanotubes destruction mechanisms

---

1. Introduction

The carbon nanotube (CNT), and in particular the single wall nanotube (SWNT), is still after almost thirty years of intense international research, a robust motor for scientific inquiries into nano and quantum science. This quintessentially one-dimensional nanoscience object possesses a variety of electrical, optical, and mechanical properties that have given birth to a legion of applications. The main hurdle for many of these applications is the localization and organization of high quality and adapted CNTs into specific architectures while preserving their superior properties, often related to their crystal quality and high aspect ratios. Thus one salient line of research that leads to specific scientific questions and applications is the search for strategies that align, select, localize and perfect SWNTs [1, 2, 3]. Applications include flexible and high-temperature electronics, optoelectronics, and thermoelectrics [4], nanofluidics [5], ultimate nanoscale transistors [6, 7], nanomechanics [8], scanning probe tips [9], quantum mechanical systems [10] and field emission (FE) sources [11].

To overcome the main hurdle through better control of growth, one would obviously firstly wish to observe the time-resolved growth of individual CNTs at the atomic scale and secondly to dispose of useful tools for controlling such growth, even dynamically if possible. For such a control, different external forces such as electric field [12], gas flow [13], interactions with atomic steps

[14] and defined crystal lattices [15] have been exerted during CVD growth to guide the growth directions of SWNTs.

The first demonstration of growth under electric field is by Zhang *et al.* [12]. They clearly showed the synthesis of single-walled nanotubes well aligned by the electric field. The same synthesis without electric field produced on the contrary nanotubes with random orientations. The syntheses were mostly carried out on substrates where the electrodes and the catalyst were deposited by lithography or other localization techniques. In this configuration, observations can only be made after growth and no estimation of growth kinetics is given. A recent remarkable result is the demonstration that electric field during growth can even be used to modify the type of nanotube (semi conducting or metallic)[16]. More precisely, they show that by reversing the direction of an electric field during the synthesis they manage to initiate a re-nucleation process of the catalyst so as to produce almost only semiconducting nanotubes. This revives the interest of electric-field-directed-synthesis (EFDS) by opening additional perspectives such as the selectivity of the type of nanotubes.

Of direct interest for our work is that growth under electric field has also been performed in field emission configurations. The link between FE and growth under field is natural since during growth the electric field at the end of the tube generally increases and can induce FE. If the emitted (and then accelerated) electrons strike a phosphorescent screen, one can directly observe the emission pattern of the emitters which is a greatly magnified FE microscopy (FEM) observation of the CNT ends. The nanotubes are grown directly on heated electrodes, covered with catalysts, which also generate the electric field. Bonard *et al.* grew multi wall carbon nanotubes (MWNTs) under FE conditions [17] on metallic wires and was able to determine the appearance of the first emitters, by measuring the FE current or FEM patterns, and their evolution during further growth. This allowed them to roughly estimate the growth rates of these CNTs. Another experiment of growth of SWNTs (or few wall nanotubes) on sharp W tips during FE allowed also direct observation of the nucleation events and as well that the nanotubes actually rotate either regularly or irregularly during growth [18]. These FE experiments allow to follow dynamically only approximately the CNT lengths and diameters and not many of their morphological features such as number of walls, bending, kinking, defaults, dimension changes, etc. This makes it very difficult to understand and quantify at the appropriate atomic level the orientation mechanism during synthesis. This highlights the interest of

observing direct growth in conventional electron microscopies.

In their first paper Zhang *et al.* [12] model their nanotubes as simple dielectric dipoles polarized by the external electric field. Theoretically this would result in relatively weak electrostatic forces and in their model the alignment due to the electric field competes with the thermal agitation. This first model has been taken up by most of the subsequent work and is used in review articles [19, 1, 2] to explain the alignment of nanotubes. In the articles on growth coupled to FE [17, 18, 20], the nanotubes are on the contrary considered as metallic where free electrons are obliged to collect at high field surface areas to reject field penetration. The resulting surface electric fields and electrostatic forces from these net charges are much more intense than in the dipolar model. Real time observation of the growth is then needed to clarify the alignment mechanism of the nanotubes.

This article describes our recently achieved breakthrough in the dynamical observation of EFDS of individual CNTs on micro-machined chip heaters in Environmental Transmission and Scanning Electron Microscopes (ETEM and SEM). This configuration allows the recording of a side-on view of the entire growths of several dozens of nanotubes simultaneously, permitting an unprecedented access to growth kinetics and their variabilities. This can be simultaneously accompanied by measurement of the FE currents emitted from the apexes of the growing CNTs. The configuration gives a unique access to the complex evolutions taking place during the growth under field: growth kinetics and their evolution for individual CNTs, mechanical tearing or FE induced destruction, competition between adhesion forces and electrostatic forces, etc.

First is presented the experimental system, the nature of the produced nanotubes and the video analysis technique used to follow the evolution of the growth rates. The second part focuses on the effect of the electric field (electrostatic force, FE) and the differences observed between low and high field regimes. In the third part the experimental observations of growth kinetics are discussed including their variabilities and time evolutions. The destruction mechanisms at high field strength are presented in a fourth part with in particular an original mechanism of field evaporation induced by the FE current. In the next section various other aspects such as nanotube loops or the growth of larger nanotubes are discussed. Finally some notable points raised by these observations and the consequences that can be drawn from this work will be discussed in more detail.

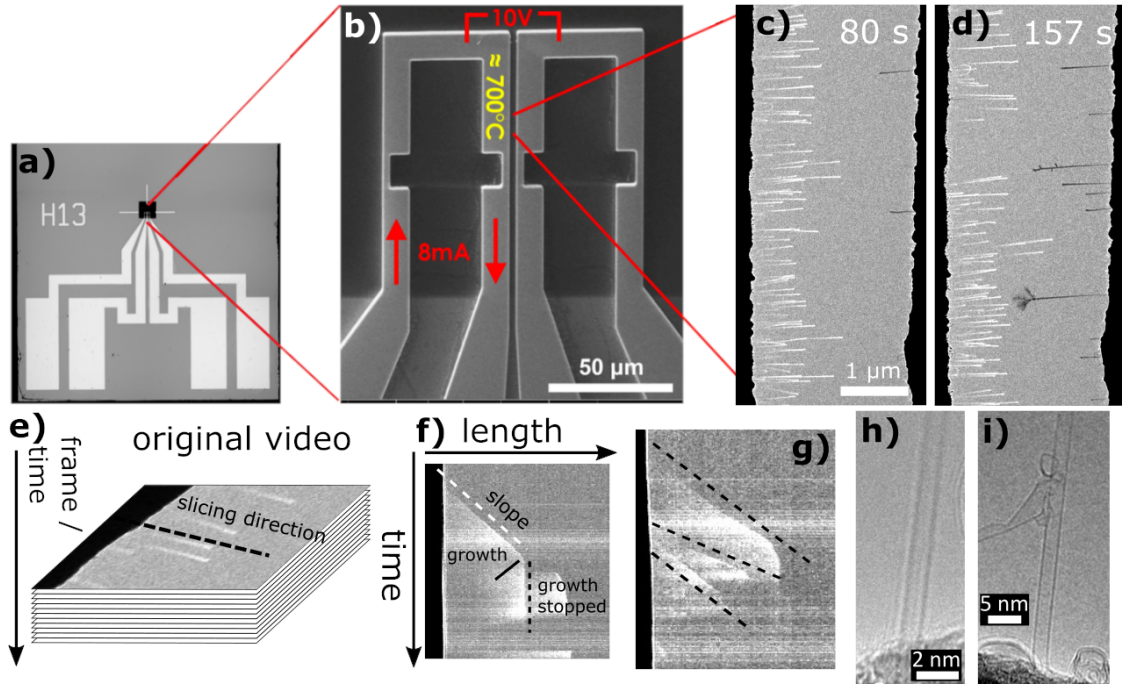

Figure 1: Electric Field Directed SWNT Synthesis in electron microscopes. a) Optical image of the micro-machined chip heater and b) SEM image of the active zone of the chip with the two cantilevers. Voltage is applied between the two cantilevers and one is heated by Joule heating. c) and d) ETEM observations of the CNT growth through the gap. In this polarity growing nanotubes appear as white straight lines parallel to the electric field. Images correspond to observations after 80 s and 157 s of growth at +50 V (see video SI-video1). The dark lines on the right in d) are nanotubes torn from the growth side that are driven by electric forces to the opposite side. e) Illustration of the obtained kymograph that allows to follow the growth kinetics of nanotubes. f) Example of a kymograph showing a growth at constant growth rate. g) Kymograph showing three successive nanotube growths. h) and i) post-growth HRTEM observation of grown nanotubes showing clean SWNTs with no apparent defects. The nanotube diameters are respectively 1 and 2,2 nm. More detailed characterization is given in S.I.3.

2. Experimental procedure and nanotube characterization.

The *in situ* growths under electric field are realized on in-house designed chips consisting of a pair of silicon cantilever heaters. The heaters are 4 μm thick and are separated by a 2 μm gap (d = 2 μm, see Fig. 1 a) and b)) [21, 22]. The cantilevers are first covered by a 5 nm alumina layer and 0.7 nm Fe thin layer in a high precision ultra-high vacuum molecular beam evaporator (MBE) system allowing the reproducible deposition of layers as thin as 0.1 nm. Both layers are deposited at room temperature directly on the heating cantilevers. The role of the alumina during the growth process is to allow the formation of nanometric Fe clusters by Oswald ripening while preventing their fast migration. Together this leads to base growth mode of small diameter nanotubes [23, 24] (all our observations of EFDS confirm exclusive base growth, see S.I.3 Fig. 3.3). The chip heater is then transferred into the TEM column and one of the two cantilevers is selected to be heated by the Joule effect for a preliminary Hydrogen pre-treatment and consecutive CNT growth (more details on sample preparation are given in Supporting Information part 2 (S.I.2)). A Keithley 6517 electro-meter applies the polarization voltage, V_{app}, to the unheated cantilevers, inducing the inter-electrode electric field ($E_0 \approx V_{app}/d$), and measures FE currents. For growth, acetylene (C_2H_2) is used as the carbon feedstock and it is mixed with a fraction of H_2 to etch amorphous carbon deposition. Gas mixture is first introduced into the TEM chamber and once the pressure stabilizes the cantilever temperature is slowly increased until roughly 650-700 °C in the growth zone (see S.I.2). In the present work, we explore the dependence of gas pressure on CNT growth rather than the temperature.

With this protocol, growth of straight CNTs is observed in the gap as shown in Fig. 1 c) (80 s) and d) (157 s) for which the applied voltage was $V_{app} = +50$ V on the unheated cantilever. The video corresponding to the 157 first seconds of synthesis is available in SI-video1. Growing nanotubes can be observed individually as bright straight lines that lengthen almost perpendicular to the gap and therefore follow the electric field lines. Note that the lateral resolution is poor during EFDS and the nanotubes are examined post growth in true HRTEM mode (no applied field) to determine their real diameters. Image contrast as a function of applied voltage and TEM setting is discussed in S.I.2. Note also that the growths are observed with very low magnification and thus low dose which explains why no influences of the beam on growths are detected. Although presently the nucleation process

is not imaged and there is a rather poor lateral resolution, many interesting observations can be made in this video which will be discussed below.

As growth is strongly oriented in the microscope's object plane, the nanotubes' growth rate, R, can be measured by the evolution of the images. This can be done by performing a kymograph visualisation as used very generally in biology. Starting from the frame stack of a video as represented in Fig. 1 e) a segment of interest is chosen (oriented along a growing nanotube) and all the frames are sliced along the same segment. Stacking these scan lines as a function of time results in a kymograph that characterizes the evolution of the nanotube's length. If the growth rate is constant as in Fig. 1 f) a straight edge is observed. Keeping this image orientation, 1/slope (or 1/angle's tangent) is proportional to the growth rate. If the growth stops a vertical edge is observed and faster growths tend toward more horizontal edges. The kymograph in Fig. 1 f) corresponds to the growth of a 515 nm long CNT during 23 seconds giving a growth rate R=22 nm/s. Note that if R is not constant the edge is not straight as we will see later. As the apex of the nanotube is particularly bright it allows to observe different nanotubes growing at the same time. Fig. 1 g) shows a kymograph where we can distinguish three successive nanotubes growing at different R's (respectively 30, 46 and 19 nm/s). The more conventional representation, length versus time, is easily obtained by a simple 90° anti clockwise rotation as illustrated in Fig. 3 j). As the nanotubes are not perfectly aligned with the object plane (for example due to the electrostatic repulsion between them) speeds can be slightly underestimated. However, considering a maximum inclination of ± 15 degrees this leads to a relative uncertainty below 5%. HRTEM observation of the grown nanotubes is performed after synthesis and confirm that nanotubes are essentially clean SWNTs with very few defects. Figs. 1 h) and i) present two individual SWNTs with diameters of 1 nm and 2.2 nm respectively. The diameters obtained by HRTEM are mostly between 0.6 and 2 nm with a mean around 1 nm. The SWNT nature was also observed by a preliminary Raman Spectroscopy study that shows clearly the presence of the expected radial breathing modes in the spectrum. More details on nanotube characterization are given in S.I.3.

3. Electric field regimes and nanotube growth kinetics.

The main original parameter of this work is the inter-electrode electric field, characterized by its intensity and direction. This "capacitor" field

is principally due to the bias potential applied to the cold cantilever with an additional Joule heating voltage drop of $\sim 4V$ present on the heated cantilever.

The nanotubes grow directly on the heated electrode of the capacitor and thus are electrically connected, possibly through a high contact resistance, with that electrode. The electric field and surface charge density on all surface elements in the gap are then obtained by solving the Laplace equation. The electric fields at the apexes of the nanotubes growing in the gap are amplified by the tip effect. The apex electric field is generally written $E_{0A} = \beta E_0$ where β is the amplification factor. For a single nanotube of radius r and length L growing between two infinite planes, $\beta \sim L/r$. Thus during growth high E_{0A} and associated electrostatic forces appear that strengthen enormously as the growth proceeds. These fields (and forces) are critical to this work.

Although large electric fields are readily generated at modest applied voltages on these nanometric objects, surprisingly few elemental charges are acquired due to the nanometric dimensions, typically 1-20 for nanotube lengths in the 100 nm range [20]. This means that the transfer of a few electrons is sufficient for the nanotubes to efficiently screen the internal electric field and generate high surface and external electric fields.

This model differs strongly from the model initially presented by Zhang *et al.* [12] which is generally repeated in the literature. As stated above, in their model the nanotube is described as a polarizable object immersed in an external field. This implies that during growth the nanotubes are perfectly isolated from the electrodes that generate the electric field and that no charge is transferred (by the surface, the gas, ...) since a few extra electrons are sufficient to screen the field. They then use the induced dipole moment of the nanotube to estimate the forces and torques applied to the nanotube.

There is an essential difference between the "isolated" (Zhang *et al.*) and "connected" (this article) configurations that must be clearly understood: the fields and forces for the former are obviously much weaker than for the later. A detailed comparison of these two configurations is given in S.I.5. As an example, for an aligned nanotube in a macroscopic field one obtains a tensile force of 0.97 pN in the isolated configuration compared to a tensile force of 5.5 nN in the connected configuration. As the isolated case leads to weak aligning electrostatic forces, thermomechanical vibrations have to be considered that can alter the nanotube alignment. In the case of connected nanotubes, the forces being thousands of times higher, these thermal vibrations are very

small and negligible. The video given in SI-video1 clearly shows as expected that thermal vibrations are negligible and very good orientation is observed even for small nanotubes. In the following the connected model is thus considered to describe our observations.

It would be of the highest utility if one could distinguish during EFDS whether a nanotube is metallic, M, or semi-conductor, SC, or even better that the electric field favours the synthesis of one of these two types. However SC-SWNTs are mostly small gap semiconductors and since growth is realized at $\sim 700°C$ they are highly conducting and thus electrically equivalent, presenting thus the same image contrast and electrical forces. This may explain why no clear signature differentiating CNT types during EFDS has yet been observed, though we do not exclude this possibility in future studies.

Large amplification factors, β, into the hundreds are obtained for the connected nanotubes during growth which has several consequences. The high apex fields can induce FE currents when they reach the 5 V/nm range and even be sufficient to modify or destroy the nanotubes. At even larger fields, field evaporation mechanisms may even appear which result in the gradual evaporation of the object. Extreme electrostatic pressure, P, develops associated with the electric field E ($P = 1/2\epsilon_0 E^2$), independent of polarity. Such forces cause bending towards the opposite electrode, an increase in mechanical resonance frequencies [25] and even tear nanotubes from their substrates. Nanotube mechanical response to these electrostatic forces also depends intrinsically on L and r. For example, the area moment of inertia, related to bending, depends on the radius to the fourth power. This explains why the effect of the electric field (alignment, stresses, etc.) will act much more effectively on small diameter nanotubes.

Now that these basic aspects have been specified, the observed behaviours during growth are discussed. It is useful to classify the growths as either "low bias" or "high bias". An example of "low bias" synthesis can be seen in SI-video2 and in Fig. 2 a) ($V_{app} = +15$ V). The main characteristics of the "low bias" regime (up to $\sim 20V$) are: i) the electric field is already sufficient to orient the growth of the SWNTs (and from the shortest lengths observable, ~ 50 nm); ii) during the growth, some nanotubes disappear probably caused by mechanical uprooting; iii) nanotubes can reach the other electrode. In this last case, some nanotubes disappear at the moment of contact while others achieve permanent contact. In this case, more and more nanotubes connected at both ends are observed. The bridging nanotubes can stick to

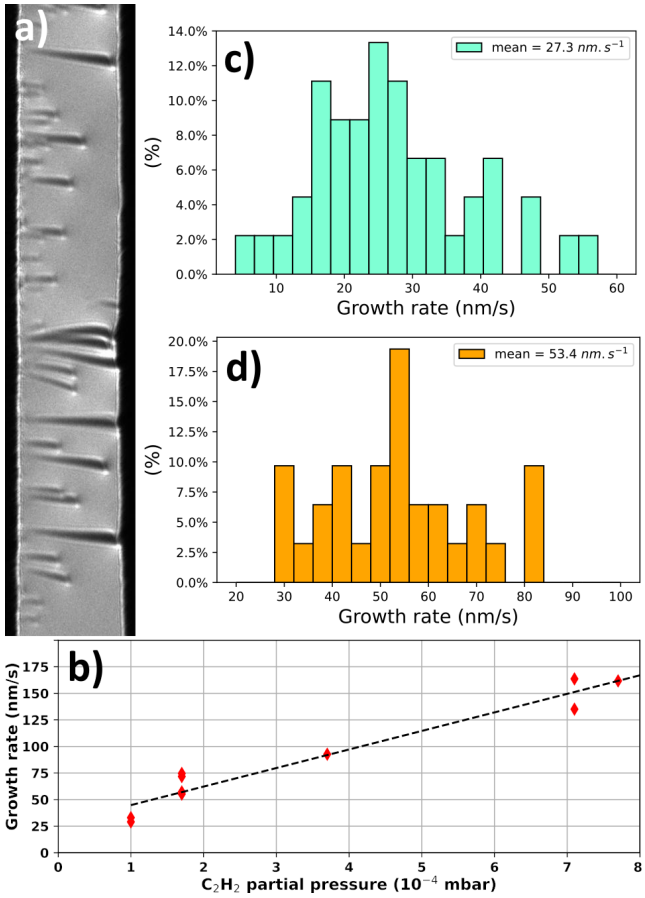

Figure 2: a) Growth observation in the "low bias" regime. Nanotubes crossing the gap are observed. Comparison can be made with the "high bias" regime illustrated in Fig.1 c) and d) in which no nanotube are connecting the other electrode. The gap is 2 μm wide. b) Evolution of the mean growth rate as a function of the C_2H_2 partial pressure. c) Nanotube growth rate histogram for the experiment corresponding to SI-video1. d) Nanotube growth rate histogram for the experiment corresponding to SI-video2.

their neighbours forming web-like structures and ropes of nanotubes that can be observed in the middle of the gap (see S.I.3 and 4). The proportion of nanotubes destroyed during contact depends on the value of the applied voltage. The fact that some tubes are not destroyed by applying $\sim$ 10-15 V (which is rather high for typical transport experiments) is perhaps due to the high contact resistance between the tubes and the substrates or even to their SC or M nature.

Note that in this "low bias" regime some nanotubes can emit electrons by FE during growth. However, the FE currents are then sufficiently weak so that they do not systematically lead to the destruction of the nanotubes before they reach the other electrode. Marchand *et al.* [18] for example followed SWNT growth using the FE patterns. However, in those experiments, the potential was gradually reduced during synthesis to maintain a constant emission current and thus prevent possible destruction mechanisms.

At strong positive polarization, "high bias regime", both electrostatic forces and FE currents become significant which we measured during several runs (see below). On the SI-video1 (+50 V polarization) it is clearly visible that many nanotubes are torn off during the growth but the most characteristic fact is that we observe no nanotube which exceeds 70% of the gap with the remaining majority reaching less than half the gap. We consider that this limitation is due to FE and associated FE-induced destruction. The precise mechanisms of destruction or degradation by FE are discussed below. Two additional proofs of the FE origin of this limitation are i) during the same synthesis, reducing the voltage to +30 V allows the next nanotubes to grow longer and ii) for growth at strong negative polarization (the same electrostatic forces apply but no FE) we actually observed many mechanical destructions but some nanotubes manage to reach the other side where they are finally destroyed during the contact.

An important parameter is the partial pressure, p, of acetylene used during synthesis. We carried out a series of experiments by varying p, the other parameters being constant and measured the average growth rate R of the nanotubes. Fig. 2 b) presents the dependence of growth rate on p. A roughly linear dependency is observed, implying pressure limited growth, at least to first order, with R varying from 30 nm/s to 160 nm/s for a p range of 10^{-4} to $7\,10^{-4}$ mbar. Consider 100 nm/s obtained for p = 4.10^{-4} mbar. The number of molecules impinging on a surface can be written as 2.63 10^{22} $(p/\sqrt{M\,T})$ $cm^{-2}.s^{-1}$, with p in mbar, M is the molar mass in grams and T the temperature in Kelvin. At this pressure, assuming T = 300 K (only the cantilever

is heated), the atomic flux is $\sim$ 1200 C_2H_2 molecules nm^{-2}.s^{-1}. This corresponds to 2400 C atoms nm^{-2}.s^{-1}, assuming a sticking coefficient of 100 %. For a 1 nm diameter CNT (125 C atoms/nm), a growth rate of 100 nm/s can be explained with a catalyst surface of 5 nm^2. This is reasonably close to the measured R. Note that the transition between pressure-limited and diffusion-limited growth has been estimated by Bonard *et al.* [17] to be $\sim$ 10^{-2} – 10^{-3} mbar.

Consider in more detail how R varies for one synthesis for different CNTs. Fig. 2 c) presents the growth rate distribution measured on more than 50 nanotubes for the synthesis corresponding to SI-video1 (acetylene p $\sim$ 10^{-4} mbar). The distribution ranges from 6.5 nm/s to 56 nm/s (ratio $\sim$ 9x) with a mean of 27.3 nm/s and a standard deviation of 11.4 nm/s. Fig. 2 d) presents the distribution for the synthesis corresponding to SI-video2 (acetylene p $\sim$ 2 10^{-4} mbar) with R ranging from 29.5 to 83 nm/s (ratio $\sim$ 3x, three times narrower than above), a mean of 53.4 nm/s and a standard deviation of 15 nm/s. These relatively large distributions are characteristic of our growth experiments. Interestingly, Otsuka *et al.* [26] and Pimonov *et al.* [27] for atmospheric pressure growth also observed very wide distributions with growth rates that can vary by up to a factor 30 between SWNTs. The source of the large range in R for fixed conditions may be the variability in active catalyst surfaces and in nanotube diameters. There is a clear interest in extending this work to include more high resolution TEM studies where the diameters and rates can be correlated. Comparison of these growth rates with other synthesis technics or conditions can be made using the review articles [2, 3, 19] that gather a lot of experimental results.

Now examine in more detail more kymographs of individual SWNTs. Firstly R is quite constant for a large majority of CNT growths as illustrated in Fig. 1 e) and f). The transitions between constant growth and end of growth is visible in the more or less pronounced rounded part between the two regimes. This transition is therefore rapid compared to the rest of the growth.

The second type of frequently observed evolution ($\sim$ 20 % of cases) corresponds to a gradual increase in R (see Figs. 3 a) and b)) leading to a more or less pronounced convexity in the kymograph. This evolution corresponds always to an increasing R (from 13 to 27 nm/s in Fig. 3 a) and from 11 to 20 nm/s for the longest nanotube in Fig. 3 b)). Generally one observes this convexity from the beginning and during all the growth interval. In much rarer cases, R accelerates later during the growth (see Figs. 3 c) and d)). In

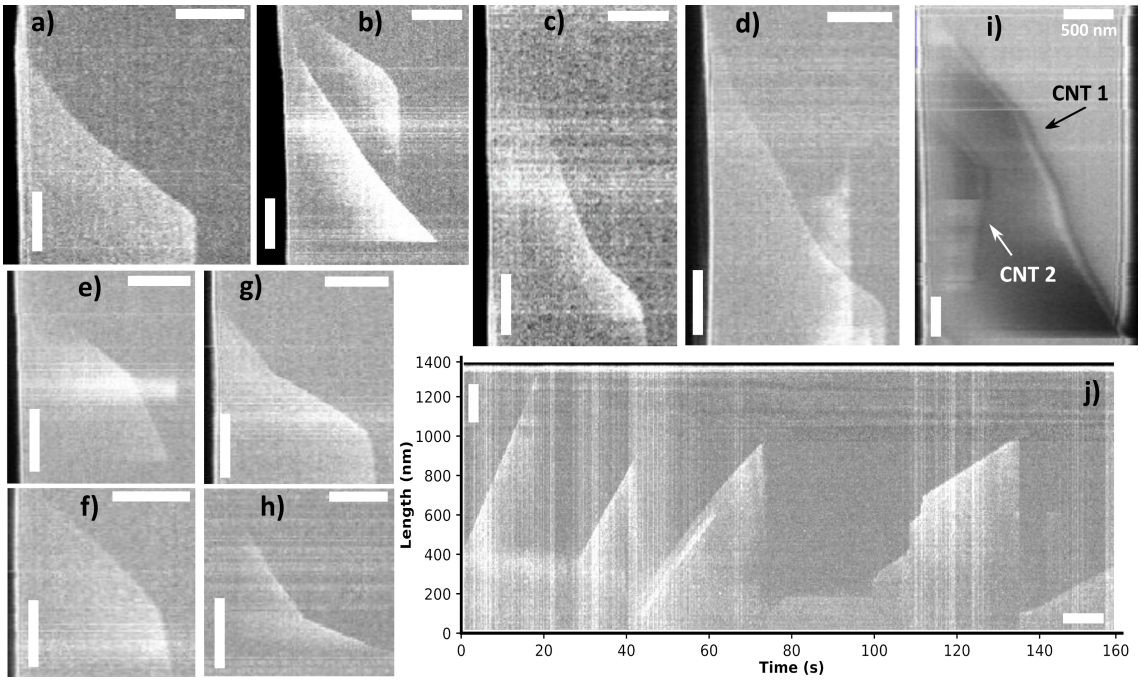

Figure 3: Different growth rate evolutions observed during synthesis. a), b) regular and gradual growth rate increases during growth. c) and d) Nanotubes showing constant growth rate followed by a rapid acceleration. e) and f) Abrupt growth rate variations, growth being linear in time before and after the transition. The transition leads to a growth rate decrease. g) and h) Other abrupt variations but leading to a growth rate increase. i) Kymograph obtained during a "low bias regime" synthesis showing the evolution of two nanotubes. CNT 1 that finally connects the opposite electrode shows different abrupt growth rates variations. For CNT 2, after a constant growth rate it shows possible shrinkage. j) 90° anti clockwise rotated kymograph of a continuously growing nanotube that regularly breaks after the acetylene gas was stopped showing gradual growth rate reduction. The different growth rates are given in the text. The horizontal scale bar corresponds to 200 nm for all images except where the value is given and the vertical scale bar corresponds to 10 s in all cases.

these cases, the beginning R seems rather constant, until the acceleration is observed (initial and maximum growth rates are respectively 10 and 30 nm/s for Fig. 3 c) and 7 and 22 nm/s in Fig. 3 d)).

Other rarer evolutions (a few percent) correspond to abrupt growth rate variations with the growth constant before and after the transition (see Figs. 3 e) to i)). These variations can be decreasing growth rates (initial and final R are 25 and 9 nm/s in Fig. 3 e) and 19 and 4 nm/s in Fig. 3 f)) or increasing growth rates (initial and final R are 16 and 33 nm/s in Fig. 3 g) and 16 and 59 nm/s in Fig. 3 h)). A more complex case (in a low bias regime growth) showing several transitions is presented in Fig. 3 i) CNT1.

To be complete, we did observe during "low bias" synthesis a few cases where after growth ended, the nanotube seems to shorten little by little (tube CNT2 in Fig. 3 i)). As the quality of the images in these syntheses is poorer and more complicated to interpret we cannot guarantee that these observations are not an artefact of imaging. For higher fields with better resolution no CNT shortening was observed.

Finally the evolution of a particularly interesting growth is presented when the acetylene supply was stopped abruptly and the gas concentration at the growth zone decreased gradually under continuous pumping (see Fig. 3 j)). A first remarkable point is that this tube breaks several times near its base but continues its growth, thus allowing us to observe successively different growth stages. The anti clockwise rotated kymograph is presented in Fig. 3 j) showing that R decreases regularly as the acetylene disappears. The average R calculated over the successive growth portions are 50, 37, 27, 13 and 10 nm/s respectively. The two abrupt jumps observed at 100-120s seem to be more related to a contact with the neighboring CNT loop which results in an apparent stop of the growth followed by a jump. The video corresponding to the growth of this nanotube is provided in SI-video3. This observation is interesting because it shows that for the same nanotube and at the same temperature the growth rate is indeed a function of the acetylene partial pressure confirming the curve obtained on Fig. 2 b) but on a single nanotube. In general this shows how EFDS in TEM allows us, to a certain measure, to play with the growth rate and length of an individual nanotube.

An interesting comparison can be made with the paper of Pimonov *et al.* [27]. In their experiments they observed a majority of constant growth rate synthesis that is also our case. Less frequently they observed growth rate variations for nearly 30 % of their nanotubes and they measured that the growth rate ratio between initial and final states was around 1.7 (or

0.6 i.e. 1/1.7). These variations correspond in our case to Figs. 3 e) to h). However in our observations this phenomenon is relatively rare and the growth rate ratios are not close to 1.7 although more statistics should be required. Interestingly, they observe that these growth rate variations do not necessarily correspond to a nanotube chirality change and indicate that the catalyst nanoparticle fluctuates between different configurations during growth. The last type of evolution they observed is a succession of growth and shrinkage, the tube being able to re-dissolve in the particle. In our case, as previously discussed, some shrinkage may occur in the "low bias" regime but have not been observed in the "high bias" regime.

Reference [27] did not report the growth acceleration phenomenon we observed. This behaviour is too clear and too frequent during our growths to be an artefact or exceptional event. As it is observed during electric field directed growth it is tempting to propose that the acceleration is induced by this electric field configuration. As stated above, the electric field at the apex increases linearly and the mechanical stress quadratically with nanotube length. At the catalyst level, the electric field is very weak because it is has a low effective height and is rapidly screened by the rest of the nanotube. However, the nanotube-catalyst interface remains subjected during synthesis to increasing stress and torque which can become very significant. These high mechanical stresses could modify the growth rate, for example by facilitating the incorporation of the later carbon atoms (by increasing the capture area for example). Though this mechanism is tempting, it should nevertheless be observed that the majority of growths occur at constant rate. So, at best, this growth acceleration would only be effective for certain types of chirality or nanotube/catalyst configuration. Another possibility is that long nanotubes that start to field emit may heat by the Joule effect, thus increasing R through an Arrhenius effect at the catalyst. This is not compatible with most of the accelerations observed because they begin near the start of the growth while the tube does not emit any FE current. On the other hand, this mechanism could explain the late accelerations observed in Figs. 3 c) and d), the acceleration only appearing when the FE becomes significant.

4. Destruction mechanisms

Another striking and important aspect in the video SI-video1 ("high bias" regime) is that a lot of growing nanotubes suddenly disappear. As previously stated, high voltages induce strong electric fields at the apex of the nanotubes

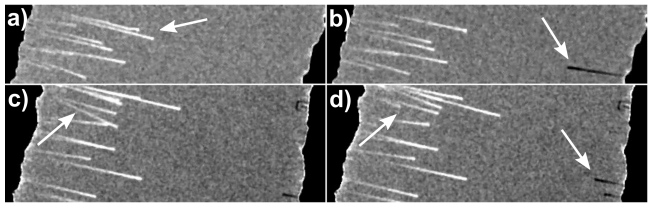

Figure 4: Destruction mechanism. a)-d) Consecutive frames of video during growth showing the fracture of CNTs and the fixation of the torn off fragment on the opposite electrode. a) and b) Images before and after the breakage of a nanotube. The entire nanotube has disappeared. c) and d) Images before and after another fracture. In d) the intact part of the torn off nanotube is still visible showing clearly a breakage along the CNT length.

that lead simultaneously to : i) high mechanical stress and ii) the possibility to extract high FE current leading to FE-induced destruction mechanisms. It is interesting to see if we can characterize and distinguish these two phenomena.

Mechanical failure is an obvious mechanism to explore since high stress can lead to the breakage of the nanotubes particularly at defects, the nanotube-catalyst contact and the catalyst support contact. One form of mechanical failure present for our EFDS is the disappearing nanotubes, immediately followed by the apparition of black lines on the opposite electrode that we call "nanodarts". Torn-off fragments or whole nanotubes are charged and thus accelerate towards the counter electrode as a dart. If the extremity can link strongly to the counter electrode, the fragment can then align along the electric field resulting in a dark contrast line. As the process is rapid compared to the video capture rate the disappearance of the tube on one side and its appearance on the other side is observable from one frame to the following. In most cases, the original nanotube totally disappears as seen in Figs. 4 a) and b) (the base of the tube near the electrode is not clearly visible). However, in some rare cases, an intact part of the tube is still visible as shown in Figs. 4 c) and d). This proves that fracture can occur along the CNT length.

The second mechanism occurs when nanotubes start to emit electrons by FE as the electric field reaches a few V/nm at the apex. In this mechanism the electric field is the most relevant parameter since it reflects the narrowing of the potential barrier at the emitter surface and governs electronic or ionic emission. Note that FE is polarization dependent but can appear here (SI-video1) because of the positive polarisation of the counter electrode. As the nanotube continues to grow, and hence the apex electric field, the FE current

can increase greatly because the current increases exponentially with electric field which to first order increases linearly with CNT length. Note that during synthesis the pressure is $\sim 10^{-4}$ mbar which is a very poor vacuum for FE that is highly sensitive to surface contamination. As a consequence, FE currents are very unstable.

At high emission current several mechanisms arise that can lead to total or partial destruction or evaporation of the tubes. These effects have been studied in the FE community as they are limiting factors for the use of nanotubes as electron sources [28]. First, as mentioned above, at high current the nanotube can heat due to resistive dissipation (intrinsic or contact resistance). Even with good electrical and thermal contacts a nanotube heats due to its intrinsic resistance along the length but for higher currents. Temperatures up to 2000 K at the apex have been measured [29]. As the current continues to increase this can lead to the destruction of the CNT at a defect. Ultimately a thermally activated field evaporation process occurs and the atoms at the apex evaporate leading to a length reduction of the nanotube [28]. It is shown below that this mechanism is observed during synthesis. The maximum FE current that a SWNT can sustain before evaporation is in the range of 100 nA to few μA depending on several parameters such as the nanotube length and the electric and thermal contacts.

Unlike conventional FE experiments where the nanotube length is given and the emission voltage is varied, here the potential is constant and the length increases during growth. If FE induced field evaporation occurs during growth, there is a competition between elongation due to growth and shortening due to evaporation. Kymographs presented in Figs. 5 a) to d) show the evolution of the lengths of several CNTs with more or less rapid length variations that we interpret as field evaporation during synthesis.

Nanotubes are initially terminated by carbon caps whose precise structure depends on the nucleation step (see S.I.3). Carbon atoms of a defect free cap are strongly bonded to their neighbours (high binding energies) so the field evaporation requires very high fields/temperatures. Once the cap is evaporated at the end of the nanotube it may maintain an open ring where the C atoms have fewer neighbours (lower binding energies) and are more easily evaporated. This would result in faster length reduction. If the extremity closes and forms a new stable cap the nanotube can continue to grow for a substantial interval before evaporation occurs again (see Figs. 5 a) and g)). On the contrary, if the formed cap is not very stable or the tube does not close, evaporation can occur more gradually during the synthesis (see

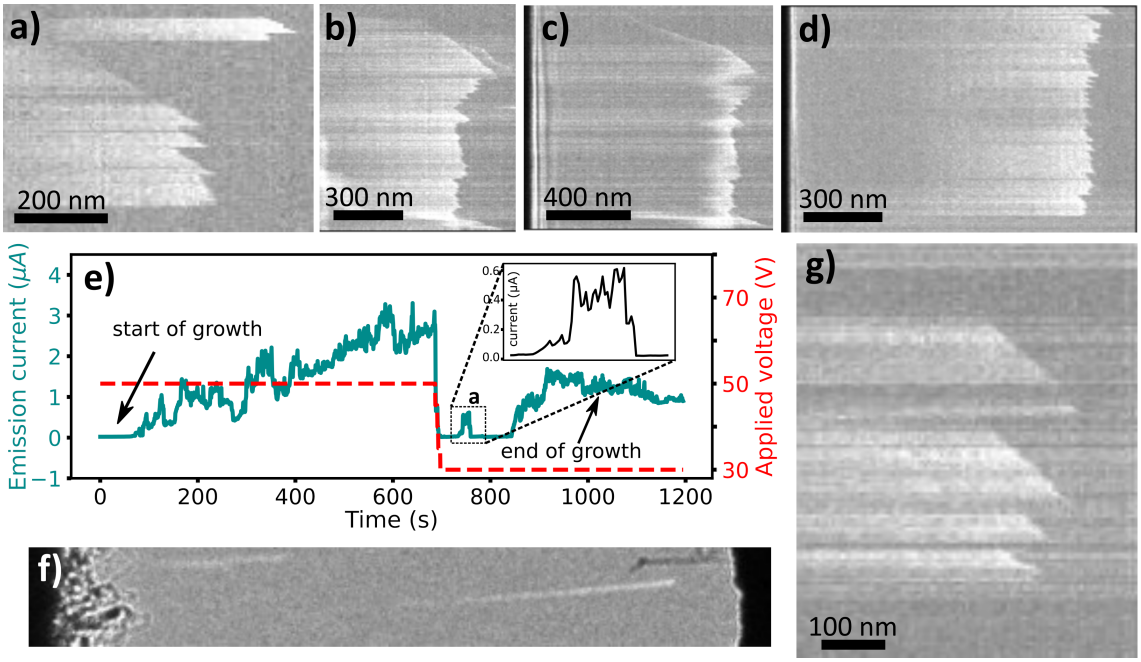

Figure 5: FE induced destruction mechanism. a)-d) Different kymographs showing more or less rugged length evolution that are interpreted as FE induced thermal evaporation of carbon nanotube during growth. e) Evolution of the global FE current and polarity during the synthesis (see text). The zone labeled "a" corresponds to the FE of the nanotube presented in f). Inset : zoom of the labeled zone "a" where an instable current of nearly 500 nA is measured before nanotube destruction. g) kymograph corresponding to the nanotube during it's emission corresponding to the FE thermal field evaporation process.

Figs. 5 b), c) and d)). Note that to assign the observed evolutions to the FE induced evaporation mechanism it is necessary to ensure that the nanotube in question emits a significant FE current.

Determination of which nanotubes are emitting is not directly possible from the video as all the CNTs are polarized. However the global FE current is measured in real time during the experiments and its evolution during the synthesis is shown in Fig. 5 e). As the voltage is kept constant at +50 V we see the global emission current increasing up to 3 μA. At this point the voltage was reduced to +30 V leading to the quasi suppression of the emitted current because the highest field potential emitter was no longer in the FE range. After a delay the emission current restarted and continued to increase because new growing CNTs with longer lengths can significantly emit.

Of note is the current increase labelled "a" in Fig. 5 e) since it corresponds to only one emitting nanotube that has been recorded and is shown in Fig. 5 f). A zoom of the current evolution is presented in the inset in Fig. 5 e) where we see a current increase up to nearly 500 nA then a more or less constant current followed by the disappearance of the emission. The video of the evolution of this nanotube is presented in SI-video4 that shows clearly the FE induced gradual destruction of this nanotube during growth with its length successively increasing and decreasing before the complete destruction of the tube. The corresponding kymograph presented in Fig. 5 g) is similar to previous ones that confirms the previous interpretations.

A remarkable point in these experiments is that we observe some nanotubes that are simultaneously growing from the base and are evaporating at the apex. In these cases it means that growth is not perturbed or inhibited by the extreme field and mechanical tension applied to the nanotube. However in our observations the concomitant growth and gradual evaporation lead finally to the total destruction of the nanotubes.

5. Nanotubes loops. Adhesion

The effect of the electric field is not limited to properly aligning the straightened nanotubes but through the forces it generates it also helps to unravel the more complex structures which tend to form under the effects of steric hindrance and adhesion.

This can be seen for example on the loops formed by thin nanotubes as presented in Figs. 6 a) and c). In these images both extremities of nanotubes are hidden at the level of the substrate or stuck on another nanotube.

In these configurations the electrostatic forces pull on the nanotube loops stretching them towards the opposing anode and even may open them. The loop form is the result of a competition between these electrostatic, adhesion and bending forces. This links these observations to the important domain of adhesion at the nanoscale. Potentially this may allow dynamic monitoring of these phenomena, during or after synthesis. Here we present a few points concerning the adhesion energies and the sliding.

Several articles present experimental measurements of adhesion energies between SWNTs and various substrates using AFM [30, 31] and binding energies between SWNTs [32] using TEM. Adhesion energy of 1.24 ± 0.11 $nJ.m^{-1}(nN)$ for example has been obtained between SWNT and clean silicon. Although there are still large discrepancies between different measurements these adhesion energies are measured in the nN range for cleaned surfaces. The opening of a nanotube loop by stretching it by an electrostatic force is quite similar to AFM experiments. During the nanotube growth the loops enlarge and go further into the gap resulting in increasing electrostatic forces. The overall electrostatic force on the loop can then reach the force needed to be pulled out. This corresponds to Figs. 6 b) and d) where we can observe the detached extremity intact and aligned to the field. However for the majority of loops the opening is followed by sudden destruction. In fact if a too long loop opens, the field and forces at the new free extremity increase so rapidly and importantly that it leads to rapid destruction.

The attachment and final configuration of nanotubes that cross the gap in the low field regime are controlled by the minimisation of total energy: electrostatic, adhesion and mechanical bending. Note that these CNTs often continue to grow after contact. The adhesion effects are better seen in post growth TEM images of the bridging CNTs (see S.I.3). The attached nanotubes are extremely straight but mostly tilted at small angles or joined together in bundles of a few nanotube. The tilting and bundling is the result of energy minimisation and in principal can be mathematically modelled.

Another interesting point is the significant number of small open loops that also often close during growth. Fig. 6 e) shows an example with an open loop (indicated by the black arrow) self-folding on itself leading to a closed loop (Fig. 6 f)). These situations probably correspond to cases where the contact of the free extremity of the tube is close to the catalyst particle making it possible to maintain a small distance between the two loop ends which are still stretched by the electric field towards the opposing electrode. During growth, thermal agitation can bring the two sides of the loop into contact

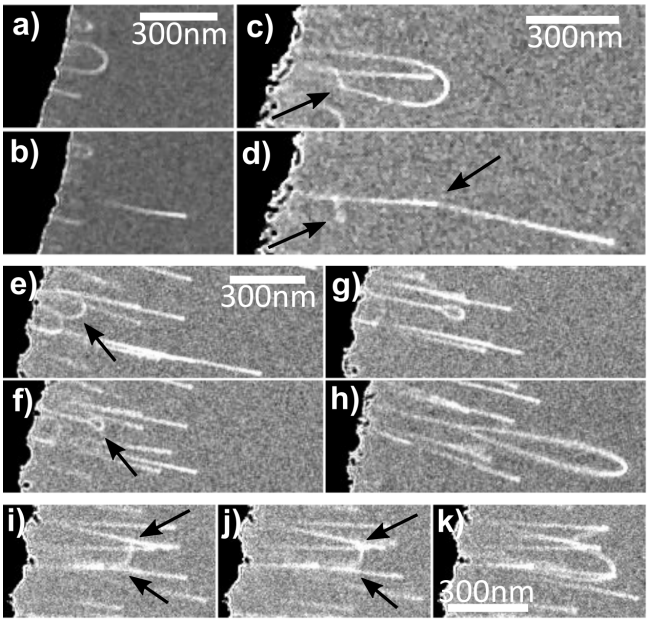

Figure 6: Evolution of nanotube loops during EFDS. a) and b) Consecutive images showing the opening of a loop whose extremity was stuck at the base. c) and d) Consecutive images showing the opening of a loop whose extremity was stuck to another nanotube. The opening is followed by the sticking to another nanotube. e) to h) Closing and evolution of a loop. e) the original open loop. f) closing of the loop with the formation of a small terminal ring resulting mainly of the balance between binding and bending energies. g) As the nanotube continues to grow the ring slightly enlarges due to increasing repulsive electrostatic energy. h) As the loop is less screened by its neighbours the ring greatly enlarges due to strong electrostatic repulsion between the two sides of the loop. i) Another loop whose two sides are stuck to two other nanotubes. Only the upper part of the loop is distinguishable forming nearly 90° angles with the two guiding nanotubes (see arrows). j) As the loop grows we observe that the two sides move forward on the guiding nanotubes indicating that electrostatic forces pull on the loop and that portions of the nanotubes are sliding on the others. k) Finally the loop detaches from its supports probably to minimize its energy.

leading to the closing of the loop. Adhesion tends to close the loop further but this is opposed by bending energy stored in the curved portion of the nanotube. The final rounded shape, sometimes named racket-like structure [33], corresponds to the energy minimization of the system. To be complete the electrostatic energy must be included in the minimisation. In Fig. 6 f) the loop is still short and probably efficiently screened by close nanotubes so the diameter of the "racket" would depend minimally on the field. From the radius of the nanotube and the shape of the racket it is then possible to estimate the binding energy per unit length, γ, of the CNT. Estimation of γ has been made using experimental observations on 4 closed loops that give values of the binding energy $\gamma \sim 0.3$ nN (see S.I.7 for details). This can be compared to the 0.36 nN obtained by Chen *et al.* [32] and theoretical values they estimated between 0.32 and 0.39 nN. In this first estimation the main uncertainties comes from the uncertainty in the diameter of the nanotubes and, to a lesser extent, the uncertainty in the projection length of the loop. However, since this is a TEM environment, these measurements can clearly be improved and dedicated experiments with HRTEM observations would provide much more accurate measurements of these binding energies.

As the growth continues (Fig. 6 g)) the final loop is constantly at the extremity showing that the electric field pulls on the loop and the walls slide over each other like pulling on a loop of yarn. The diameter of the final loop has barely increased showing that the electrostatic energy is still minor. The situation changes radically in Fig. 6 h) where the loop overtakes its neighbours and a strong widening of the loop is observed. The shape is now given by a balance between binding energy and electrostatic energy.

The sliding of nanotubes over each other induced by the electrostatic forces is even more visible in Fig. 6 i) -k). We see a loop whose two edges adhere to two neighboring nanotubes. Only the part connecting the two sides is visible forming an almost perpendicular segment between the two nanotubes (the points contact angles are indicated by arrows). During the growth, we observe that this segment rises on the two sides of the neighboring nanotubes, which implies that a part of the growing nanotube, drawn by the electrostatic force, slides on the support nanotubes. Finally, we observe that the loop is released from its two ends forming an independent open loop to minimize its total energy.

All these effects, loop opening, electrostatic repulsion between tubes, stretching of nanotubes, reduce the formation of tangled structures with thin nanotubes. The contrast is striking with the matted structure composed of

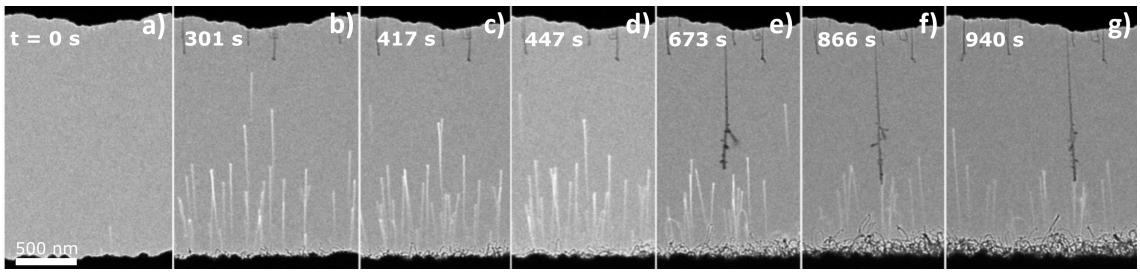

Figure 7: a)-g) Successive images of the same zone of the sample showing the formation of a foam at the base of the heated cantilever. This matted structure is composed of MWNTs and carbonaceous filaments that are not aligned by the electric field. Ultimately this foam could be an obstacle for the oriented growth of new SWNTs.

thick MWNTs that slowly grows on the electrode and that is presented in Fig. 7. HRTEM observations confirm that they are larger multi-walled nanotubes and carbonaceous filaments with many defects. As these nanotubes are larger and more rigid, they are therefore less sensitive to electrostatic forces. These nanotubes form a sort of slowly growing foam that can be seen gradually thickening at the base of the synthesis electrode as can be clearly seen on the different images of Fig. 7. If initially they do not interfere with the aligned growth of fine nanotubes, when the foam becomes too thick it is undoubtedly becoming an obstacle to the oriented growth of new nanotubes.

6. Discussion and Perspectives

The observations above clearly show how EFDS allows the growth of SWNTs aligned in the direction of the field. For thin nanotubes the orientation is obtained already at low field strength due to the generated electrostatic forces. Above two very different models ("connected" and "isolated") have been proposed to explain EFDS. Previously in the article (and in S.I.5) we have shown that these two configurations lead to different forces and torques of several orders of magnitude. The observations and experimental results presented here clearly show that only the "connected" configuration can explain the obtained phenomena. The "isolated" configuration with its dipolar model so often presented does not fit our experiments or the existing literature and must be, at least, completely revisited with clearer experiments where the electrical isolation of the nanotubes is clearly demonstrated. The dipolar approach leads to affirmations in review articles such as: *Second, the electric field directed growth is not applicable to SWNTs with diameters*

smaller than 1.4 nm which always grow in wavy configurations in electric fields regardless of their lengths.[2]. Our observations clearly prove that such claims are completely erroneous.

Another interesting point to discuss here concerns the different phenomena and nanoscale modifications at the interface or at the base of the nanotube during growth. By the base of the nanotube we obviously mean the contact zone between the nanotube and the catalyst but this can include more generally the catalytic particle and its possible evolutions as well as the contact between the catalyst and the barrier layer.

A first point concerns the orientation of SWNTs by the electric field. Images of long nanotubes strongly curved by the application of electric field are quite commonly used to demonstrate the extraordinary flexibility and strength of these nano-objects (see for example S.I.6). In these cases the upper part is almost perfectly aligned while a strong curvature is observed closer to the base which ends at the rigid contact where very strong mechanical torques and tensions exist. We consider that the alignment of our thin nanotubes can be more pronounced during the synthesis when the temperature is high and the catalyst active. For a nanotube originally growing in a different direction than the field direction the electrical forces result in high forces and torques at the interface. Energetically speaking, the minimal configuration corresponds to the nanotube aligned along its entire length in the direction of the field. It seems very likely that energetically guided modifications (rotation of the catalyst, atomic diffusion accompanied by displacement of the common CNT-catalyst edge, ...) can lead to an alignment of the tubes at the base of the nanotube. These scenarios can be compared to the observations made *in situ* on the beginning of SWNT nucleation as for example [34] (see S.I.6). In these very nice observations one can see for example a rather free catalyst particle which rotates and seems to move slightly on the support during the growth. Other images show particles firmly anchored on the support but whose surface planes change. These observations seem to indicate that modifications at the base of the nanotubes can allow an alignment in the field axis at the base itself.

A second aspect concerns the destruction of nanotubes. We observe an important number of ripped off nanotubes leading to their complete disappearance. As mentioned above, we also observe some partial breakage of nanotubes but these cases are in the minority. At the same time other nanotubes show a phenomenon of field evaporation which proves that some nanotubes can withstand extremely strong pulling conditions without being

destroyed or torn off. It would be interesting to know if these destructions occur at the contact between the CNT and the catalytic particle or if the particle itself is torn off during the destruction. Once again the observations made by Chao *et al.* [34] are interesting because they show two very different states of catalyst. As previously discussed, in the first case the catalyst seems to be mobile on the support and one can easily suppose that for relatively weak forces the catalyst can be ripped from the support, leading to the destruction of the nanotube. In the second case the catalyst seems to be firmly anchored onto the support and even if atomic modifications can appear the particle should be able to resist very strong mechanical stresses.

Discuss now how these results could have ramifications for fundamental reserach and applications. Complementary theoretical and experimental studies of the beginning of the synthesis and the evolution of the nanotube base during the synthesis could open new avenues in SWNT growth control. In our synthesis, the growth rate being proportional to the partial pressure, it is possible to lower the rate to observe the growth dynamics in more detail. This could allow us to see the effect of alignment on the nanotubes at its base and to understand the destruction or tearing mechanisms. We are currently working on modified microchips to obtain transparent areas for the electron beam. A post-growth HRTEM image is presented in S.I.3 showing observation of the substrate/catalyst/nanotube base. The image contains one large, clean SWNT and a beginning of a short mulitwall nanotube, both with their catalytic particles. Though certainly challenging this suggests that HRTEM during EFDS is quite possible in our system. These experiments may lead to the realization of original samples for various applications. It was shown that the 'low bias regime' allows to obtain oriented nanotubes connected to the other electrode. For the optimization of the growth it is interesting to determine the minimum voltage allowing a good orientation of the tubes while minimizing the risks of destruction of some nanotubes during the contact. In contrast the synthesis of singly connected, or suspended SWNTs, is interesting for example for the realization of field emission electron cathodes or advanced near field probes. In this case the growth in the 'high bias' regime seems promising. For example on Fig.1 c), corresponding to 80 s of synthesis, we observe many oriented nanotubes which stop more or less in the middle of the gap (about 1 micron), this length limitation being ultimately due to the field emission mechanism. If these nanotubes were preserved while other nanotubes were growing leading to a gradual increase of the nanotube density, this synthesis technique would immediately constitute the grail for the

realization of a high brightness electron cathode.

Finally, these first *in situ* growth experiments allow us to envisage many complementary experiments with other synthesis conditions coupled with other characterization techniques. A first important point obviously concerns a better characterization of the SWNTs produced to determine their metallic or semiconductor character and potentially their chirality. These studies can for example be performed by HRTEM, electron diffraction and Raman spectroscopy to test if the growth under field is accompanied by a certain selectivity for example in terms of nature or chirality.

7. Conclusion

These studies have allowed for the first time the *in situ* ETEM dynamic observation of the growth of individual SWNTs under electric field. The electric field leads to extremely straight aligned nanotubes that in turn allows unprecedent growth rate measurements and growth rate variation observations on tens of SWNTs simultaneously. Depending on the electric field intensity and direction, different regimes are observed leading to SWNTs crossing the gap or SWNTs length limited in the gap. Furthermore these measurements allow to clarify the mechanisms involved in the orientation of fine nanotubes and invalidate the widespread dipole model for growth under field. The ETEM with heated microchip constitutes a versatile, ideal platform to study systematically the synthesis and evolution of nanotubes while offering opportunities for complementary electrical, thermal and mechanical measurements.

Acknowledgements

Authors acknowledge financial support from the French state managed by the National Research Agency through the projects NanoMAX (ANR-10-EQPX-50), 3DX ONline(ANR-15-CE08-0002) and Solitube (ANR-22-CE09-0005). The authors thank the Centre Interdiscipinaire de Microscopie Electronique de l'Ecole Polytechnique (CIMEX), the Plateforme Nanofils et Nanotubes Lyonnaise of the University Lyon and the METSA (Microscopie Electronique et Sonde Atomique) network.

References

[1] A. Corletto, J. Shapter, Nanoscale patterning of carbon nanotubes: Techniques, applications, and future, Adv. Sci. 8 (2021) 2001778.

[2] M. He, S. Zhang, J. Zhang, Horizontal single-walled carbon nanotube arrays: Controlled synthesis, characterizations, and applications, Chem. Rev. 22 (2020) 12592.

[3] X. Q. Li, P. X. Hou, C. Liu, H. M. Cheng, Preparation of metallic single-wall carbon nanotubes, Carbon 147 (2019) 187.

[4] W. Gao, N. Komatsu, L. Taylor, G. V. Naik, K. Yanagi, M. Pasquali, J. Kono, Macroscopically aligned carbon nanotubes for flexible and high- temperature electronics, optoelectronics, and thermoelectrics, J. Phys. D: Appl. Phys. 53 (2020) 063001.

[5] E. Seechi, S. Marbach, A. Niguès, D. Stein, A. Siria, L. Bocquet, Massive radius-dependent flow slippage in carbon nanotubes, Nature 537 (2016) 201–213.

[6] Q. Cao, Carbon nanotube transistor technology for more-moore scaling, Nano Research 14 (2021) 3051–3069.

[7] D. Tang, S. Erohin, D. Kvashnin, V. Demin, A. Cretu, S. Jiang, L. Zhang, P. Hou, G. Chen, D. Futaba, Y. Zheng, R. Xiang, X. Zhou, F. Hsia, N. Kawamoto, M. Mitome, Y. Nemoto, F. Uesugi, M. Takeguchi, S. Maruyama, S. Cheng, Y. Bando, C. Liu, P. Sorokin, D. Golberg, Semiconductor nanochannels in metallic carbon nanotubes by thermomechanical chirality alteration, Science 374 (2021) 1616–1620.

[8] C. Urgell, W. Yang, S. De Bonis, C. Samanta, M. Esplandiu, Q. Dong, Y. Jin, A. Bachtold, Cooling and self-oscillation in a nanotube electromechanical resonator, Nature Physics 16 (2020) 32–37.

[9] B. Cheng, S. Yang, W. Li, S. Li, S. Shafique, D. Wu, S. Ji, Y. Sun, Z. Jiang, Controlled growth of a single carbon nanotube on an afm probe, Microsyst. Nanoeng. 7 (2021) 80.

[10] A. Baydin, F. Tay, J. Faan, M. Manjappa, W. Gao, J. Kono, Carbon nanotube devices for quantum technology, Materials 15 (2022) 1535.

[11] Y. E. Saito, Carbon Nanotube and Related Field Emitters: Fundamentals and Applications, ISBN: 978-3-527-32734-8, 2010.

[12] Y. Zhang, A. Chang, J. Cao, Q. Wang, W. Kim, Y. Li, N. Moriis, E. Yenilmez, J. Kong, H. Dai, Electric-field-directed growth of aligned single-walled carbon nanotubes, Appl. Phys. Lett. 79 (2001) 3155.

[13] A. Cassell, N. Franklin, T. Tombler, E. Chan, J. Han, H. Dai, Directed growth of free-standing single-walled carbon nanotubes, J. Am. Chem. Soc. 121 (1999) 7975.

[14] V. Derycke, R. Martel, M. Radosavljevic, P. Avouris, Catalyst-free growth of ordered single-walled carbon nanotube networks, Nano Lett. 2 (2002) 1043.

[15] S. Han, X. Liu, C. Zhou, Template-free directional growth of single-walled carbon nanotubes on a- and r-plane sapphire, J. Am. Chem. Soc. 127 (2005) 5294.

[16] J. Wang, X. Jin, Z. Liu, G. Yu, Q. Ji, H. Wei, J. Zhang, K. Zhang, D. Li, Z. Yuan, J. Li, P. Liu, Y. Wu, Y. Wei, J. Wang, Q. Li, L. Zhang, J. Kong, S. Fan, K. Jiang, Growing highly pure semiconducting carbon nanotubes by electrotwisting the helicity, Nature Catalysis 1 (2018) 326.

[17] J. Bonard, M. Croci, C. Klinke, F. Conus, I. Arfaoui, T. Stockli, A. Chatelain, Growth of carbon nanotubes characterized by field emission measurements during chemical vapor deposition, Phys. Rev. B 67 (2003) 085412.

[18] M. Marchand, C. Journet, D. Guillot, J. Benoit, B. Yakobson, S. Purcell, Growing a carbon nanotube atom by atom :"and yet it does turn", Nano Lett. 9 (2009) 2961.

[19] R. Zhang, Y. Zhang, F. Wei, Horizontally aligned carbon nanotube arrays: growth mechanism, controlled synthesis, characterization, properties and applications, Chem. Soc. Rev. 46 (2017) 3661.

[20] A. Pascale-Hamri, S. Perisanu, A. Derouet, C. Journet, P. Vincent, A. Ayari, S. T. Purcell, Ultrashort single-wall carbon nanotubes reveal field-emission coulomb blockade and highest electron-source brightness, Phys. Rev. Lett. 112 (2014) 126805.

[21] C. Kallesøe, C.-Y. Wen, K. Mølhave, P. Bøggild, F. M. Ross, Measurement of local si-nanowire growth kinetics using in situ transmission electron microscopy of heated cantilevers, Small 6 (2010) 2058–2064.

[22] F. Panciera, M. Norton, S. Alam, S. Hofmann, K. Mølhave, F. M. Ross, Controlling nanowire growth through electric field-induced deformation of the catalyst droplet, Nat. Commun. 7 (2016) 12271.

[23] H. Yoshida, S. Takeda, T. Uchiyama, H. Kohno, Y. Homma, Atomic-scale in-situ observation of carbon nanotube growth from solid state iron carbide nanoparticles, Nano Lett. 8 (2008) 2082–2086.

[24] R. Sharma, E. Moore, P. Rez, M. M. Treacy, Site-specific fabrication of fe particles for carbon nanotube growth, Nano Lett. 9 (2009) 689–694.

[25] S. Purcell, P. Vincent, C. Journet, V. Binh, Tuning of nanotube mechanical resonances by electric field pulling, Phys. Rev. Lett. 89 (2002) 276103.

[26] K. Otsuka, S. Yamamoto, T. Inoue, B. Koyano, H. Ukai, R. Yoshikawa, R. Xiang, S. Chiashi, S. Maruyama, Digital isotope coding to trace the growth process of individual single-walled carbon nanotubes, ACS Nano 12 (2018) 3994.

[27] V. Pimonov, H. N. Tran, L. Monniello, S. Tahir, T. Michel, R. Podor, M. Odorico, C. Bichara, V. Jourdain, Dynamic instability of individual carbon nanotube growth revealed by in situ homodyne polarization microscopy, Nano Lett. 21 (2021) 8495.

[28] K. Dean, T. Burgin, B. Chalamala, Evaporation of carbon nanotubes during electron field emission, Appl. Phys. Lett. 79 (2001) 1873.

[29] S. Purcell, P. Vincent, C. Journet, V. Binh, Hot nanotubes: Stable heating of individual multiwall carbon nanotubes to 2000 k induced by the field-emission current, Phys. Rev. Lett. 88 (2002) 105502.

[30] J. Buchoux, L. Bellon, S. Marsaudon, J.-P. Aimé, Carbon nanotubes adhesion and nanomechanical behavior from peeling force spectroscopy, Eur. Phys. J. B 84 (2011) 69.

[31] T. Li, A. Ayari, L. Bellon, Adhesion energy of single wall carbon nanotube loop on various susbstrates, J. Appl. Phys. 117 (2015) 164309.

[32] B. Chen, M. Gao, J. Zuo, S. Qu, B. Liu, Y. Huang, Bending of parallel carbon nanotubes, Appl. Phys. Lett. 83 (2003) 3570.

[33] A. E. Cohen, L. Mahadevan, Kinks, rings, and rackets in filamentous structures, Proceedings of the National Academy of Sciences 100 (2003) 12141–12146.

[34] H.-Y. Chao, H. Jiang, F. Ospina-Acevedo, P. B. Balbuena, E. I. Kauppinen, J. Cumings, R. Sharma, A structure and activity relationship for single-walled carbon nanotube growth confirmed by in situ observations and modeling, Nanoscale 12 (2020) 21923–21931.